Space-Time Spectral Analysis and its Applications to Atmospheric Waves

By Yoshikazu Hayashi

Geophysical Fluid Dynamics Laboratory/NOAA, Princeton University
Princeton, New Jersey 08540, U.S.A.
(Manuscript received 19 September, 1981)

Abstract

Space-time spectral analysis methods and their applications to large-scale atmospheric waves are reviewed.

Space-time spectral analysis resolves transient waves into eastward and westward moving components and is mathematically analogous to rotary spectral analysis which resolves two-dimensional velocity vectors into clockwise and anticlockwise components. Space-time spectral analysis can also resolve transient waves consisting of multiple wavenumbers into standing and traveling wave packets. Space-time energy spectra are governed by space-time spectral energy equations which consist of linear and nonlinear energy transfer spectra.

Space-time spectra can be estimated by either the lag correlation method, direct Fourier transform method or the maximum entropy method depending on the length of the time record. By use of the modified space-Fourier transform these spectra can be estimated correctly from polar-orbiting satellite data which are sampled globally at different hours of the day.

Space-time spectral analysis has been extensively applied to data generated by GFDL general circulation models to determine the wave characteristics, structure and energetics of transient planetary waves, to verify the model with observations and to clarify their generation mechanisms by means of controlled experiments.

1. Introduction

In theoretical studies the equations of motions governing atmospheric disturbances are linearized and solved for space-time Fourier components to examine their wavenumber-frequency relation, amplitude-phase structure and energetics. In order to interpret observed and simulated disturbances in terms of theoretical wave modes, it is helpful to analyze these disturbances into space-time Fourier components. However, due to the stochastic nature of atmospheric waves, their space-time Fourier components are random variables and are not in themselves statistically and physically meaningful. For this reason space-time spectral analyses have been developed to obtain statistically meaningful results from a given space-time series which is cyclic in space and limited in time.

These analyses have been extensively applied to data generated by general circulation models to determine the wave characteristics, structure and energetics of transient disturbances which can then be compared with those observed. Generation mechanisms of these waves can also be studied by means of further controlled experiments.

In Section 2 methods of space-time spectral analysis are reviewed[1] in the following order.

- 2.1 Space-time spectral formulas
- 2.2 Estimation by the maximum entropy method
- 2.3 Estimation from polar-orbiting satellite data
- 2.4 Space-time spectral energy equations
- 2.5 Analogy with rotary spectra
- 2.6 Partition into standing and traveling waves
- 2.7 Analysis of wave packets

1 The greater part of this article has been reported in Japanese in *Tenki*, 1980, Vol. 27, No. 11, 783-801.

Section 3 gives some examples of applications of space-time spectral analysis to simulated and observed waves. Remarks are given in Section 4.

2. Methods of space-time spectral analysis

It is assumed that a given space-time series is cycle in longitude (x) and limited in time ($0<t<T$). For convenience, a discrete representation is used for frequencies (ω) as well as wavenumbers (k).

2.1 *Space-time spectral formulas*

The space-time series $w(x, t)$ is expanded into a space-time Fourier series as

$$W(x,t)=R_e\sum_{k,\omega}[\hat{W}_{k,\omega}e^{i(kx+\omega t)} +\hat{W}_{k,-\omega}e^{i(kx-\omega t)}], \quad (1)$$

where $\hat{W}_{k,\omega}$ is the complex space-time transform determined by

$$2\hat{W}_{k,\omega}=\frac{1}{\pi T}\int_0^T\left[\int_0^{2\pi}W(x,t)e^{-ikx}\right]e^{-i\omega t}\,dt, \quad (2)$$

Here, the positive and negative frequencies correspond to westward and eastward phase velocities respectively, for positive k.

The space-time power spectrum $P_{k,\omega}$ is defined as the variance of the space-time Fourier component of (1) and is given by

$$P_{k,\omega}(W)=\frac{1}{2}\langle|\hat{W}_{k,\omega}|^2\rangle, \quad (3)$$

where $<\ >$ denotes the ensemble mean which, in practice, is replaced by a frequency band mean by virtue of ergodicity. As the data length becomes longer the band width can be reduced.[2]

Kao (1968) estimated space-time power spectra by direct use of eq. (3). However, his estimates were not statistically meaningful, since a frequency band mean was not taken, as was pointed out by Hayashi (1973), Tsay (1974) and Pratt (1976).

On the other hand, Hayashi (1971, 1977b, 1981b)'s method enables one to estimate space-time cross spectra by use of time spectral analysis methods such as the lag correlation method, the direct Fourier transform method and the maximum entropy method depending on the length of the record. These methods give not only power spectra and cospectra as given by Kao's method, but also phase difference and coherence. Izawa (1972) estimated space-time cross spectra by use of a two-dimensional lag correlation method. This method is not computationally efficient for planetary-scale waves but is suitable for localized waves.

The following describes Hayashi's method for estimating space-time cross spectra.

Eqs. (1) and (2) can be written as

$$W(x,t)=\sum_k F_k(t)e^{ikx} \quad (4a)$$

$$=\sum_k[C_k-iS_k(t)]e^{ikx} \quad (4b)$$

$$\hat{W}_{k,\omega}=\frac{1}{T}\int_0^T F_k(t)e^{-i\omega t}\,dt \quad (5a)$$

$$=\hat{F}_k/2 \quad (5b)$$

$$=[\hat{C}_k-i\hat{S}_k]/2, \quad (5c)$$

where $F_k(t)$ is the space complex Fourier coefficient and $\hat{F}_k$ is its time complex Fourier transform. $C_k(t)$ and $S_k(t)$ are the cosine and sine space coefficients and $\hat{C}_k$ and $\hat{S}_k$ are their time complex Fourier transforms.

Insertion of (5b) and (5c) into (3) gives the following formula

$$4P_{k,\pm\omega}(w)=P_{\pm\omega}(F_k) \quad (6a)$$

$$=P_\omega(C_k)+P_\omega(S_k)\pm 2Q_\omega(C_k,S_k), \quad (6b)$$

where P_ω and Q_ω are the time power and quadrature spectra of a complex (or real) time series.

It follows from (6b) that

$$P_{k,\omega}(w)+P_{k,-\omega}(w)=[P_\omega(C_k)+P_\omega(S_k)]/2, \quad (7)$$

and

$$P_{k,\omega}(w)-P_{k,-\omega}(w)=Q_\omega(C_k,S_k). \quad (8)$$

According to (8), the quadrature spectrum between the cosine and sine coefficients can be interpreted as the difference between the space-time power spectra of eastward and westward moving components. Since the cosine and sine coefficients of traveling waves are 90° out of phase,[3] Deland (1964, 1972) interpreted the quadrature spectrum as indicating the amplitude square of traveling waves, while its sign indicates the direction of phase propagation. Thus the space-time power spectral formula (6b) is a generalization of Deland's method.

More generally, space-time cross spectra between two sets of time series (w, w') are formulated as

2 When the lag correlation method is used, a larger lag implies a smaller frequency band width.

3 The reverse is not necessarily true in the presence of standing wave oscillations.

$$4K_{k,\pm\omega}(w,w') = K_{\pm\omega}(F_k, F_k') \quad (9a)$$
$$= K_\omega(C_k, C_k') + K_\omega(S_k, S_k')$$
$$\pm Q_\omega(C_k, S_k') \mp Q_\omega(S_k, C_k'), \quad (9b)$$
$$4Q_{k,\pm\omega}(w,w') = Q_{\pm\omega}(F_k, F_k') \quad (10a)$$
$$= \pm Q(C_k, C_k') \pm Q_\omega(S_k, S_k')$$
$$- K_\omega(C_k, S_k') + K_\omega(S_k, C_k'), \quad (10b)$$

$$Ph_{k,\pm\omega}(w,w') = \tan^{-1}[Q_{k,\pm\omega}(w,w')/K_{k,\pm\omega}(w,w')], \quad (11)$$

and

$$\mathrm{Coh}^2_{k,\pm\omega}(w,w') = \frac{K^2_{k,\pm\omega}(w,w') + Q^2_{k,\pm\omega}(w,w')}{P_{k,\pm\omega}(w) P_{k,\pm\omega}(w')}, \quad (12)$$

where K, Q, Ph, Coh denote cospectra, quadrature spectra, phase difference and coherence.

2.2 *Estimation by the maximum entropy method*

Space-time cross spectra can be estimated from sufficiently long time records by using either the lag correlation method or the direct Fourier transform method (see Jenkins and Watts, 1968; Bendat and Piersol, 1971). When the length of a time record is short or the time variation of a wave amplitude is to be studied, the maximum entropy method (MEM) applied to the space-time spectral formulas in complex representation gives a space-time cross spectra with fine frequency resolutions (Hayashi, 1977b, 1981b).

In principle, the MEM power spectral distribution is determined by extrapolating the known lag correlations to an infinite lag in such a way that the entropy (a measure of information) is maximized. In practice, the MEM power spectra are estimated by extrapolating the available data to an infinite length of time by fitting an autoregressive process. More generally, the MEM cross spectra are estimated by fitting a multivariate autoregressive process. For reviews of the MEM, the reader is referred to Ulrych and Bishop (1975), Hino (1977) and Childers (1978).

Fig. 1 compares space-time cross spectra of given sinusoidal waves, of 5 and 20 day periods plus white noise, which are estimated by the lag correlation method with a 10 day lag and the MEM from a data set of 30 days of daily data. It is seen that the MEM gives sharper spectral peaks than the lag method.

2.3 *Estimation from polar-orbiting satellite data*

It takes one day for a polar orbiting satellite

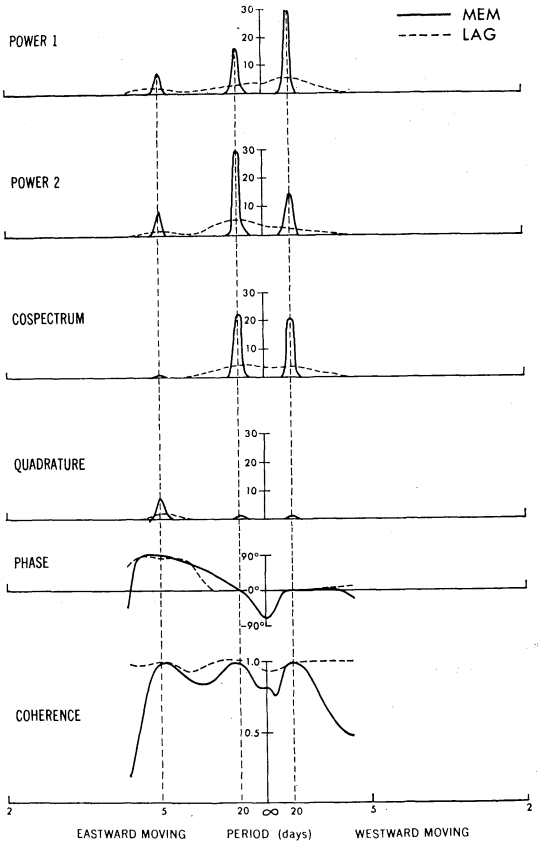

Fig. 1 Space-time cross spectra of sinusoidal waves (wavenumber 1, period 5 and 20 days) with white noise estimated from a time series of 30 days of daily data by the maximum entropy method (solid) and lag correlation method (dashed) with a 10 day lag. (After Hayashi, 1981b).

to collect data along a latitude circle. This time difference causes significant errors in the computed space-time spectra for periods shorter than 10 days as shown by Fig. 2 (top). This error cannot be eliminated by linearly interpolating data to the same time as can be seen in Fig. 2 (middle). However, this error can be completely eliminated for any selected period (4 days, eastward, for example) as shown in Fig. 2 (bottom) by the method proposed by Hayashi (1980b). This method is based on the fact that the time difference shifts the true wavenumber by ω/Ω where Ω is the angular velocity of the earth. It can be proven that the time-cross spectra of the space-Fourier transform $F_{k,\omega}$ with respect to the frequency-shifted wavenumber give the correct space-time cross spectra for the particular frequency. In practice, $F_{k,\omega}$ can be computed as

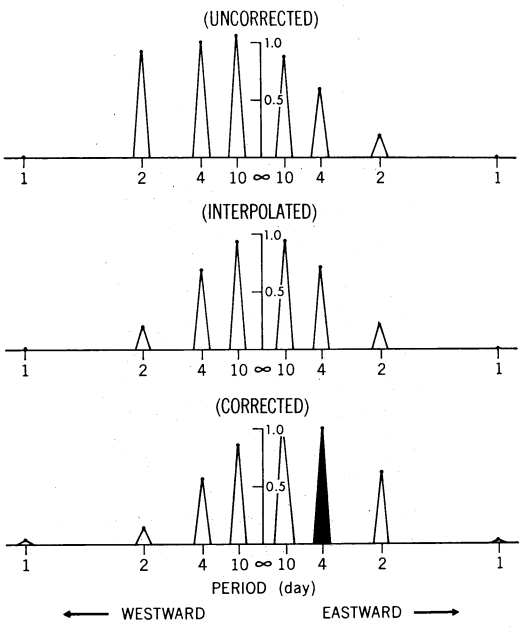

Fig. 2 The ratio of the space-time power spectra (wavenumber 1) at the equator estimated from artificial polar-orbiting satellite data to the peak value of artificial ground measured data. Standing wave oscillations are given which consist of both eastward and westward moving components with wavenumber 1 and multiple periods of 10, 4, 2, 1 days. Top: Without correction. Middle: With linear interpolation of data. Bottom: Corrected with respect to eastward 4-day period peak (shaded). (After Hayashi, 1980c).

$$F_{k,\,\omega}(t)=C_{k,\,\omega}(t)-iS_{k,\,\omega}(t)\,, \tag{13}$$

where

$$C_{k,\,\pm\omega}(t)=\pi^{-1}\int_0^{2\pi}[w\cos(fx)]\cos(kx)dx \pm\pi^{-1}\int_0^{2\pi}[w\sin(fx)]\sin(kx)dx\,, \tag{14}$$

and

$$S_{k,\,\pm\omega}(t)=\mp\pi^{-1}\int_0^{2\pi}[w\sin(fx)]\cos(kx)dx +\pi^{-1}\int_0^{2\pi}[w\cos(fx)]\sin(kx)dx\,, \tag{15}$$

with $f=\omega/\Omega$.

2.4 Space-time spectral energy equations

The space-time spectral energy equations can be obtained by generalizing the wavenumber spectral energy equations (Saltzman, 1957) which are reformulated by Hayashi (1980a) as

$$\partial K_n/\partial t=\langle K_0\cdot K_n\rangle+\langle K_m\cdot K_n\rangle-P_n(\alpha,\omega) -[\partial P_n(\phi,v)/\partial y+\partial P_n(\phi,\omega)/\partial p] +[P_n(u,F_u)+P_n(v,F_v)]\,, \tag{16}$$

and

$$\partial A_n/\partial t=\langle A_0\cdot A_n\rangle+\langle A_m\cdot A_n\rangle+P_n(\alpha,\omega) +(\nu/c_p)P_n(T,J)\,. \tag{17}$$

In the above equations, K_n and A_n are the kinetic and available potential energies for wavenumber n components, respectively. K_n is given by

$$K_n=[P_n(u,u)+P_n(v,v)]/2\,, \tag{18}$$

where $P_n(a,b)$ denotes the wavenumber cospectrum between a and b given by the space Fourier transform of a and b as

$$P_n(a,b)=\frac{1}{2}R_e\hat{a}\hat{b}\,. \tag{19}$$

Also, $-P_n(\alpha,\omega)$ is the conversion of A_n into K_n. $P_n(\phi,v)$ and $P_n(\phi,\omega)$ are the meridional and vertical fluxes of energy, respectively. $P_n(u,F_u)$ and $P_n(v,F_v)$ are the zonal and meridional components of energy dissipation, respectively. $(\nu/C_p)P_n(T,J)$ is the thermal production or destruction of A_n.

The linear energy transfer spectra $\langle K_0.K_n\rangle$ represents the transfer of kinetic energy to the wavenumber n component by interaction between the mean flow and the wavenumber n component. The explicit expression is given by

$$\langle K_0\cdot K_n\rangle=-\left[\frac{\partial u_0}{r\partial\theta}P_n(u,v)+\frac{\partial v_0}{r\partial\theta}P_n(v,v)\right] -\frac{\tan\theta}{r}[u_0P_n(u,v)-v_0P_n(u,u)] -\left[\frac{\partial u_0}{\partial p}P_n(u,\omega)+\frac{\partial v_0}{\partial p}P_n(v,\omega)\right] -\left[\frac{\partial v_0K_n}{\partial y}+\frac{\partial\omega_0K_n}{\partial p}\right], \tag{20}$$

where the suffix 0 denotes the zonal mean.

The nonlinear energy transfer spectra $\langle K_m.K_n\rangle$ represents the transfer of kinetic energy to the wavenumber n component by interaction among different wavenumber components. The explicit expression is given by

$$\langle K_m\cdot K_n\rangle=-\left[P_n\left(u,\frac{\partial u'u'}{\partial x}\right)+P_n\left(v,\frac{\partial u'v'}{\partial x}\right)\right] -\left[P_n\left(u,\frac{\partial u'v'}{\partial y}\right)+P_n\left(v,\frac{\partial v'v'}{\partial y}\right)\right] +\frac{\tan\theta}{r}[P_n(u,u'v')-P_n(v,u'u')] -\left[P_n\left(u,\frac{\partial u'\omega'}{\partial p}\right)+P_n\left(v,\frac{\partial v'\omega'}{\partial p}\right)\right], \tag{21}$$

where the prime denotes the deviation from the zonal mean.

In Hayashi's formulation the nonlinear products such as uv are regarded as a single variable. In Saltzman's (1957) formulation, the space-Fourier transform of a nonlinear product of two variables u, v is computed as the product sum (convolution) $\sum_m \hat{u}_m^* \hat{v}_{n+m}$ of the space-Fourier transform $\hat{u}_n$, $\hat{v}_n$ of the two variables.

The space-time spectral energy equations can be formulated by replacing the wavenumber cospectra in the above equations by space-time cospectra. In this case the left hand sides of (16) and (17) vanish, since the amplitude of the space-time Fourier components is constant in time.

It is important here to remark that the space-time spectral energy equations formulated above differ from those formulated by Kao (1968) and applied by Kao and Lee (1977) not only in the methods of computing the space-time spectra but also in their physical interpretations. As pointed out by Hayashi (1982), Kao's formulation cannot be interpreted as physically describing how the space-time spectral energy is maintained, although his equation is mathematically correct. Kao's (1968) spectral energy equation should not be confused with the time-Fourier decomposition of wavenumber spectral energy equations as formulated by Kao (1980) to analyze the evolution of wavenumber energy spectra.

2.5 *Analogy with rotary spectra*

Space-time spectra are mathematically analogous to rotary spectra (see Mooers, 1973, Hayashi, 1979a). As formulated by (6a), space-time spectra can be interpreted as the time spectra of a complex wave vector F_k, while the rotary spectra are the time spectra of a complex rotary vector $w=u+iv$.

As illustrated by Fig. 3 the eastward and westward rotations of the wave vector correspond to the clockwise and anticlockwise rotations of the rotary vector. One period corresponds to one rotation of the vectors. Standing wave oscillations consisting of eastward and westward moving components correspond to rectilinear oscillations consisting of clockwise and anticlockwise rotating components.

The rotary coherence between clockwise and anticlockwise components $Coh_\omega(w, w^*)$ is related (see Hayashi, 1979a) to the coherence between u and v as

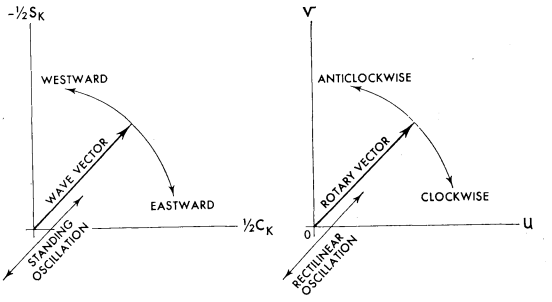

Fig. 3 Wave vector (left) and rotary vector (right) in a complex plane. The directional angles of these two vectors represent phase angle and rotational angle, respectively. (After Hayashi, 1979).

$$[1-\mathrm{coh}_\omega^2(w, w^*)]P_\omega(w)P_{-\omega}(w) = [1-\mathrm{coh}_\omega^2(u, v)]P_\omega(u)P_\omega(v), \quad (22)$$

If the rotary coherence is 1, the clockwise and anticlockwise components interfer with each other perfectly to form elliptic or rectilinear two-dimensional oscillations. If this coherence is 0, the oscillations are irregular or circular.

The degree of rectilinear oscillation L_ω is defined (Hayashi, 1979a) as

$$L_\omega = \frac{2P_\omega^{1/2}(w)P_{-\omega}^{1/2}(w)}{P_\omega(w)+P_{-\omega}(w)}\mathrm{coh}_\omega(w, w^*). \quad (23)$$

The oscillations are rectilinear for $L_\omega=1$ and irregular or circular for $L_\omega=0$.

The degree of polarization D_ω (see Born and Wolf, 1975) is related (Hayashi, 1979a) to the rotary coherence as

$$(1-D_\omega^2)=\frac{4P_\omega(w)P_{-\omega}(w)}{[P_\omega(w)+P_{-\omega}(w)]^2} \times[1-\mathrm{coh}_\omega^2(w, w^*)]. \quad (24)$$

The oscillations are polarized (elliptic, circular or rectilinear) for $D_\omega=1$ and unpolarized (irregular) for $D_\omega=0$.

The following inequality holds (Hayashi, 1979a) for the above three quantities as

$$L_\omega \leq \mathrm{coh}_\omega(w, w^*) \leq D_\omega. \quad (25)$$

Space-time spectra can be combined with rotary spectra to resolve space-time rotary vector series into eastward and westward as well as clockwise and anticlockwise components (Hayashi, 1979a). As shown in Fig. 4, the wind vector of westward moving waves rotates clockwise (anticlockwise) on the northern (southern) side of the center of vortices. The rotary spectral analysis can be used to infer the direction of the propagation of vortices when data are

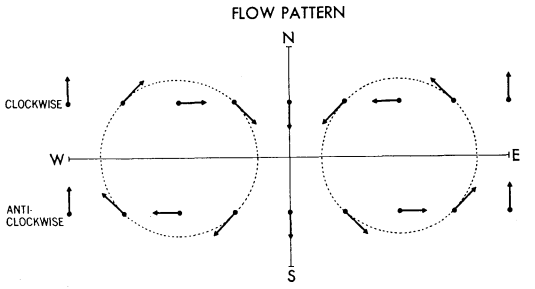

Fig. 4 Flow vectors of vortices. When these vortices travel westward, the vectors on the northern (southern) side rotate clockwise (anticlockwise). (After Hayashi, 1979a).

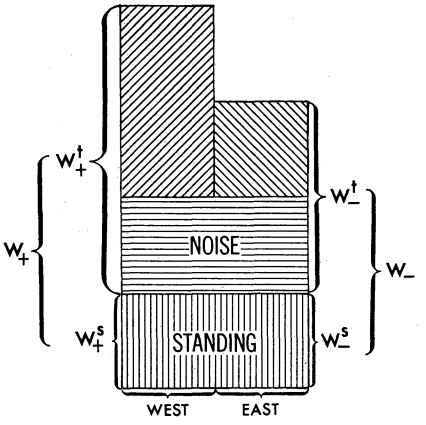

Fig. 5 Schematic diagram of standing ($w_{\pm}{}^s$) and traveling ($w_{\pm}{}^t$) components. See text for explanation. (after Hayashi, 1979b)

available at only one station.

2.6 Partition into standing and traveling waves

Standing wave oscillations are mathematically decomposed into eastward and westward components by a space-time Fourier analysis and are sometimes difficult to distinguish from other traveling waves. In order to overcome this difficulty, Hayashi (1977a, 1979b) proposed a method of partitioning space-time power spectra into standing and traveling wave parts. This method is based on the following definitions and assumptions (see Fig. 5).

i) Standing part (w^s) is defined as consisting of eastward and westward moving components ($w_{\pm}{}^s$) which are of equal amplitude and are coherent.

ii) Traveling part (w^t) is defined as consisting of eastward and westward moving components ($w_{\pm}{}^t$) which are incoherent with each other. This part also contains irregular and noise components.

iii) It is assumed that standing and traveling parts are of a different origin and are incoherent with each other.

Space-time power spectra can be partitioned as

$$P_{k,\omega}(w)+P_{k,-\omega}(w) = P_{k,\omega}(w^s)+[P_{k,\omega}(w_+{}^t)+P_{k,\omega}(w_-{}^t)], \quad (26)$$

where the spectra on the right-hand side are determined from

$$P_{k,\omega}(w^s)=2P_{k,\omega}{}^{1/2}(w)P_{k,-\omega}{}^{1/2}(w) \times \mathrm{coh}_\omega(w_k, w_{-k}), \quad (27)$$

and

$$P_{k,\omega}(w_{\pm}{}^t)=P_{k,\pm\omega}(w) -P_{k,\omega}{}^{1/2}(w)P_{k,-\omega}{}^{1/2}(w)\mathrm{coh}_\omega(w_k, w_{-k}). \quad (28)$$

Here, $Coh_\omega(w_k, w_{-k})$ denotes coherence between the eastward and westward moving components[4] and is determined by

$$4[1-\mathrm{coh}_\omega{}^2(w_k, w_{-k})]P_{k,\omega}(w)P_{k,-\omega}(w) =[1-\mathrm{coh}_\omega{}^2(C_k, S_k)]P_\omega(C_k)P_\omega(S_k) \quad (29a)$$

When MEM is used, this coherence should be computed as

$$\mathrm{coh}_\omega(w_k, w_{-k})=\mathrm{coh}_\omega(F_k, F_k{}^*), \quad (29b)$$

and $P_{k,\pm\omega}$ should be computed as part of the MEM cross spectra between F_k and $F_k{}^*$ for consistency.

Eq. (27) is reduced by use of (29) to the "standing variance" defined by Pratt (1976). When the assumption (iii) does not hold or the coherence is overestimated due to the finite length of a time record, Eq. (28) can give a negative value of power spectra.

Recently, Shäfer (1979) proposed a method of partitioning space-time power spectra into "wave" and "noise" parts. This partition is based on the assumption that the eastward and westward moving components of the "wave" are of the same origin and coherent, while those of the "noise" are of the same amplitude and are incoherent with each other. This partition is analogous to that of rotary spectra into polarized and unpolarized parts (see Hayashi, 1979a).

On the other hand, Iwashima and Yamamoto

4 The coherence between C_k and S_k depends on the origin of the coordinate. Its maximum value D_ω is given by

$$(1-D_\omega{}^2)=\frac{4P_\omega(C_k)P_\omega(S_k)}{[P_\omega(C_k)+P_\omega(S_k)]^2}[1-\mathrm{coh}_\omega{}^2(C_k, S_k)]$$

(1971) proposed a method of resolving a space-Fourier component into standing and traveling components by use of time filtering. This method is based on the assumption that the node of standing wave oscillations coincides with the zero point of time mean waves.

2.7 Analysis of wave packets

In order to discuss the longitudinal distribution of wave amplitude, waves must be treated as wave packets consisting of multiple wavenumbers.

Wave packets with wavenumber band Δk are expressed by

$$W_{\Delta k}(x,t)=R_e\sum_{\Delta k}W_k(t)e^{ikx} \tag{30a}$$

$$=R_e a(x,t)e^{i\phi(x,t)}, \tag{30b}$$

where a and ϕ are the envelope and phase functions defined (Hayashi, 1981a) by

$$a(x,t)=|\sum_{\Delta k}W_k(t)e^{ikx}| \tag{31a}$$

$$=(c^2+s^2)^{1/2}, \tag{31b}$$

and

$$\phi(x,t)=\arg\{\sum_{\Delta k}W_k(t)e^{ikx}\} \tag{32a}$$

$$=-\tan^{-1}(s/c), \tag{32b}$$

Here, c and s are the real and imaginary parts of the complex Fourier series and are defined by

$$c(x,t)=\sum_{\Delta k}[C_k(t)\cos(kx)+S_k(t)\sin(kx)], \tag{33}$$

and

$$s(x,t)=\sum_{\Delta k}[-C_k(t)\sin(kx)+S_k(t)\cos(kx)]. \tag{34}$$

Fig. 6 shows an example of an envelope defined by eq. (31). For high wavenumbers the envelope agrees with the local amplitude defined as the square root of the local spatial variance.

By generalizing the method in Section 2.1, the time power spectrum of wave packets $W_{\Delta k}$ estimated at various locations can be partitioned (Hayashi, 1979b) as

$$P_\omega(w_+ + w_-)=P_\omega(w_+)+P_\omega(w_-)+2K_\omega(w_+,w_-), \tag{35}$$

where $w_\pm$ is a wave packet consisting of either westward or eastward moving components.

The spectra on the right-hand side of eq. (35) are found by

$$P_\omega(w_\pm)=[P_\omega(c)+P_\omega(s)\pm 2Q_\omega(c,s)]/4, \tag{36}$$

$$K_\omega(w_+,w_-)=[P_\omega(c)-P_\omega(s)]/4, \tag{37}$$

and

$$Q_\omega(w_+,w_-)=K_\omega(c,s)/2. \tag{38}$$

The third term (cospectra) on the right-hand side of (35) represents interference between eastward and westward moving components. This term vanishes when it is zonally averaged or when the coherence between the eastward and westward components is zero.

On the other hand, by generalizing the method in Section 2.6, the time power spectra of wave packets are partitioned (Hayashi, 1979b) as

$$P_\omega(w_+ + w_-)=P_\omega(w^s)+[P_\omega(w_+{}^t)+P_\omega(w_-{}^t)], \tag{39}$$

where w^s is a standing wave packet, $w_\pm{}^t$ is the westward (or eastward) component of a traveling wave packet.

The spectra on the right-hand side of eq. (39) are determined by the following formulas:

$$P_\omega(w^s)=2P_\omega{}^{1/2}(w_+)P_\omega{}^{1/2}(w_-)\mathrm{coh}_\omega(w_+,w_-)\times\{1+\cos[Ph_\omega(w_+,w_-)]\}, \tag{40}$$

$$P_\omega(w_\pm{}^t)=P_\omega(w_\pm)-P_\omega{}^{1/2}(w_+)P_\omega{}^{1/2}(w_-)\times\mathrm{coh}_\omega(w_+,w_-), \tag{41}$$

and

$$\mathrm{coh}_\omega{}^2(w_+,w_-)=[K_\omega{}^2(w_+,w_-)+Q_\omega{}^2(w_+,w_-)]/P_\omega(w_+)/P_\omega(w_-), \tag{42}$$

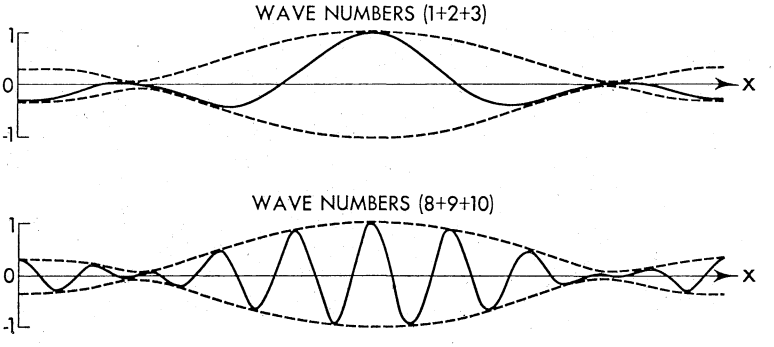

Fig. 6 Example of a wave packet. Solid curves indicate $R_e\sum_k \exp(ikx)$, while dashed curves indicate its envelope computed as $|\sum_k \exp(ikx)|$,

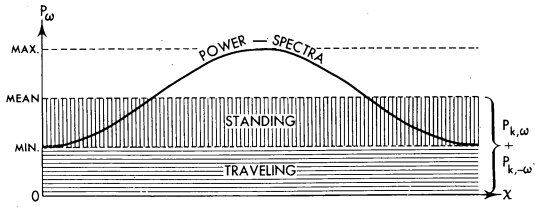

Fig. 7 Spacial distribution of the time power spectra (solid curve) of disturbances composed of eastward and westward moving waves with a single wavenumber and the same frequencies. The space-time power spectrum of a traveling wave component (including noise) is equal to the minimum value of the time power spectrum. The space-time power spectrum of a standing wave component is equal to the difference between the space mean time power spectrum and that of the traveling wave component. (After Hayashi, 1977a).

$$Ph_\omega(w_+, w_-) = \tan^{-1}[Q_\omega(w_+, w_-)/K_\omega(w_+, w_-)]. \quad (43)$$

For a single wavenumber, eq. (39) coincides with eq. (26) when it is averaged zonally (see Fig. 7).

3. Applications to atmospheric waves

The space-time spectral analyses have been applied to simulations (Hayashi, 1974; Hayashi and Golder, 1977, 1980) and control experiments (Hayashi and Golder, 1978) of large-scale tropical and mid-latitude waves generated by the GFDL general circulation grid and spectral models developed by Manabe *et al.* (1974, 1979). Space-time spectral analysis methods developed by the author have also been applied to observed data by Gruber (1974), Zangvil (1975), Hartmann (1976), Sato (1977), Fraedrich and Böttger (1978), Shäfer (1979), Pratt (1977, 1979), Venne and Stanford (1979), Pan (1979), Böttger and Fraedrich (1980), Krishnamurti (1979), Krishnamurti and Ardanuy (1980), Depradine (1980, 1981), Zangvil and Yanai (1980, 1981), Straus and Shukla (1981) and Miyakoda *et al.* (1981). In this section some of the highlights of the above papers are given as examples of the applications of a space-time spectral analysis to large-scale atmospheric waves.

3.1 *Analysis of equatorial waves*

Fig. 8 shows the space-time power spectra (6b) of a GFDL grid general circulation model's meridional component at 110 mb over the equator during the period July-August.[5] The lag correlation method with a lag of 15 days was used. The spectral peak at wavenumber 4 and westward moving period of 4.5 days corresponds to observed mixed Rossby-gravity waves discovered observationally by Yanai and Maruyama (1966).

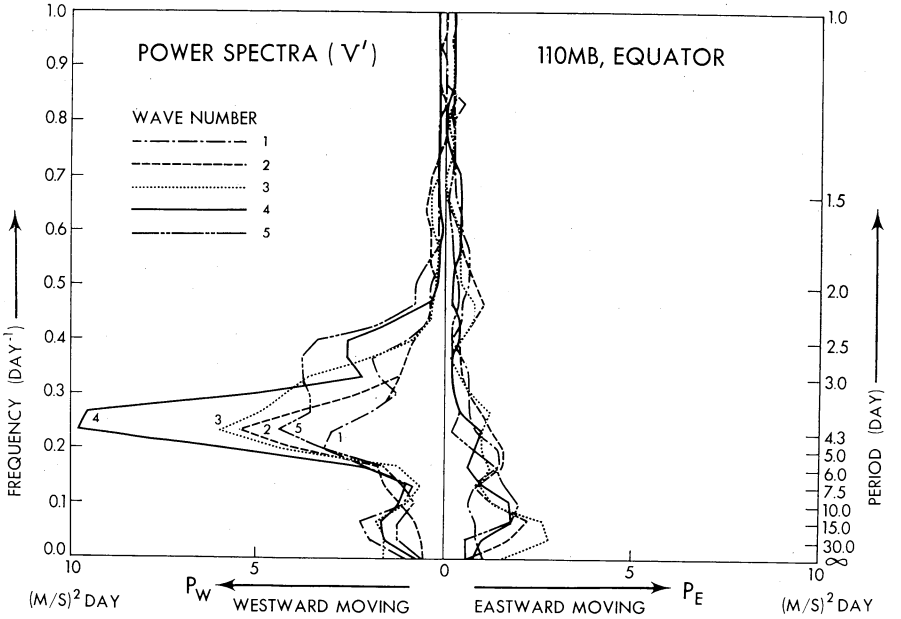

Fig. 8 Space-time power spectra of the grid model's meridional component at 110 mb over the equator during the period July August.

5 In Hayashi (1974), power spectra during the period July-October were presented.

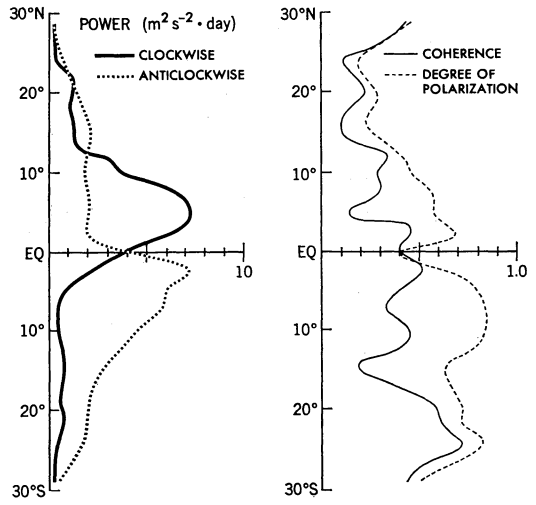

Fig. 9 Latitudinal distributions (grid model, 110 mb, June-September) of the space-time rotary power spectrum (left), rotary coherence and degree of polarization (right) for wavenumber 4, period 4 days (westward moving), frequency band with 0.05 day^{-1}. (After Hayashi, 1979a).

The latitudinal distribution in Fig. 9 shows a space-time rotary power spectrum (wavenumber 4, period 4 days, westward moving), rotary coherence and degree of polarization (see Section 2.5) of the model's wind at 110 mb. Since the streamlines of mixed Rossby-gravity waves are centered on the equator, their rotary spectra are dominated by clockwise and anticlockwise components in the northern and southern hemispheres, respectively. The degree of polarization, which is a measure of elliptic oscillations is larger than the coherence between the clockwise and anticlockwise components as expected from eq. (25).

Fig. 10 shows the vertical distribution of the space-time power spectra (wavenumber 4, period 4.3 days, westward moving) of the model's meridional component, vertical phase difference given by eq. (11) and coherence given by (12). The phase line tilts eastward in the troposphere and westward in the stratosphere, in agreement with observed mixed Rossby-gravity waves.

The geographical distribution (Fig. 11) shows the time power spectrum (period, 3~6 days, westward moving) of the model's meridional component at 110 mb consisting of wavenumbers 3~5 as computed by use of the formula (36). It is seen that mixed Rossby-gravity waves attain their largest time amplitude over the equatorial Pacific.

Fig. 12 shows the height-longitude distribution at the equator of the power spectrum described in Fig. 11. In the troposphere, the maximum time amplitude occurs over the western Pacific and shifts its position eastward with height in the direction of their upward-eastward group velocity.

Fig. 13 gives the wavenumber-frequency distribution (0~1,000 mb, 10°S~20°N) of energy conversion ($-\overline{\alpha'\omega'}$) from eddy available potential energy into eddy kinetic energy and the meridional convergence of energy flux ($-\partial\overline{\phi'v'}/\partial y$) computed by use of (9b). It is seen that the

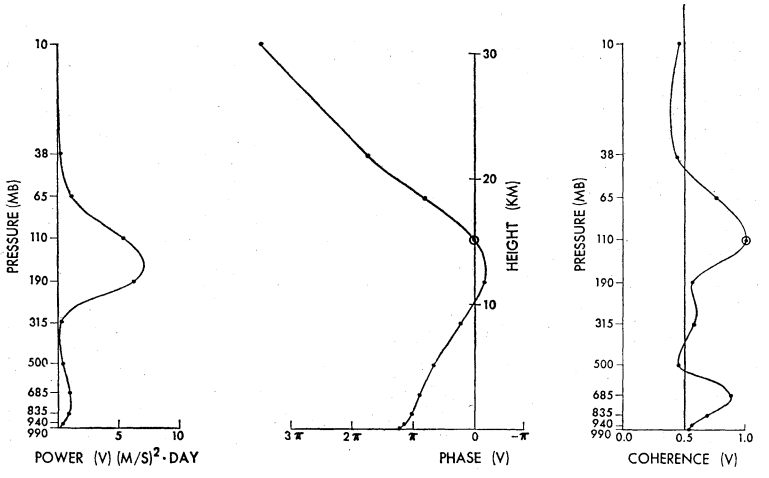

Fig. 10 Vertical distribution (grid model, equator, July-October) of the space-time power spectra (wavenumber 4, period 4.3 days, westward moving) of the meridional component phase difference and coherence with respect to 110 mb level. (After Hayashi, 1974).

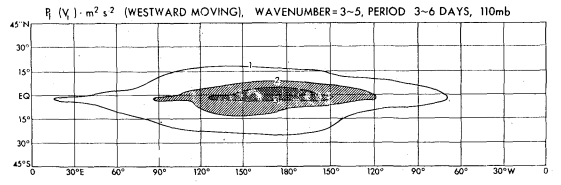

Fig. 11 Geographical distribution (grid model, 110 mb, April-September) of the time power spectrum (period 3~6 days, westward moving) of the meridional component consisting of wavenumbers 3~5.

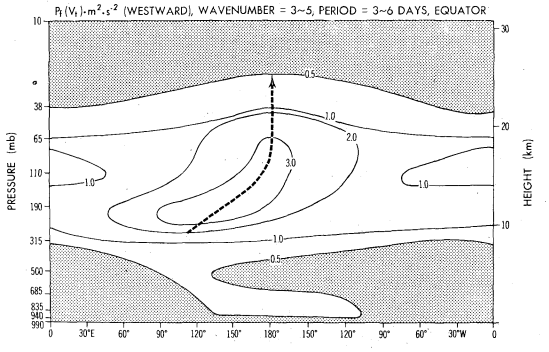

Fig. 12 Height-longitude distribution (grid model, equator, April-September) of the time power spectrum (period 3~6 days, westward moving) of the meridional component consisting of wavenumbers 3~5. The dashed line indicates the zonal maximum of the power spectrum.

former energy spectra have larger values than the latter for wavenumbers 3~5 and westward moving periods of 4~5 days. This implies that energetically the effect of condensational heating is more important than the lateral energy flux in maintaining mixed Rossby-gravity waves.

The upper part of Fig. 14 shows a latitude-time section at 110 mb of the MEM power spectrum (wavenumbers 3~5) of the model's meridional component for westward moving periods of 3~6 days computed by use of (6a). It is seen that mixed Rossby-gravity waves over the equator attain their largest amplitude around July, weaken and then regain their amplitude around January. For a wider period range (3~20 days), as illustrated by the lower panel of Fig. 14, the seasonal variation of the amplitude of these equatorial waves seems, to some extent, to be influenced by mid-latitude disturbances.

Space-time spectral analysis is also a powerful tool to analyze the results of control experiments. The latitude-time sections at 98 mb in Fig. 15 gives the MEM power spectrum (wavenumber

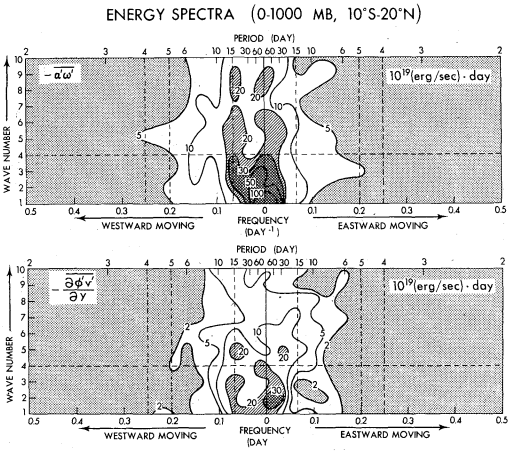

Fig. 13 Wavenumber-frequency distribution (grid model) of the energy conversions (0~1,000 mb, 10°S~20°N, July-October). (After Hayashi, 1974).

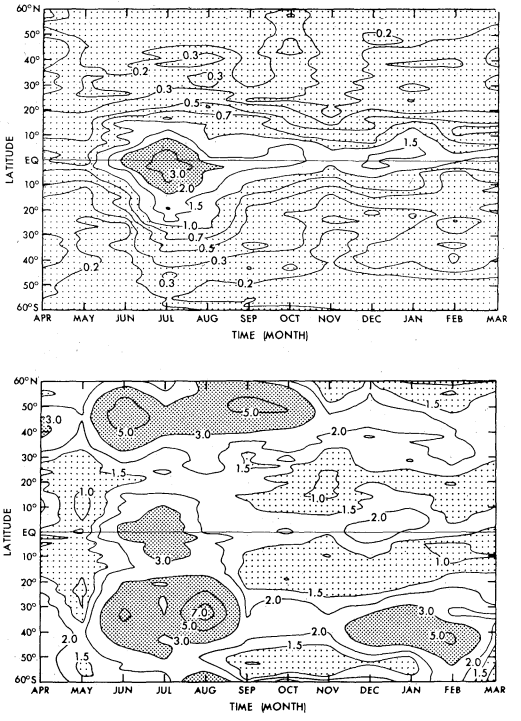

Fig. 14 Latitude-time section (grid model, 110 mb) of the MEM power spectrum (wavenumbers 3~5) of the meridional component for westward moving periods of 3~6 days (upper) and 3~20 days (lower). (After Hayashi and Golder, 1980).

3~5, periods 4~15 days, westward moving) of the model's meridional component. Small random disturbances are initially given on June 1 (left)

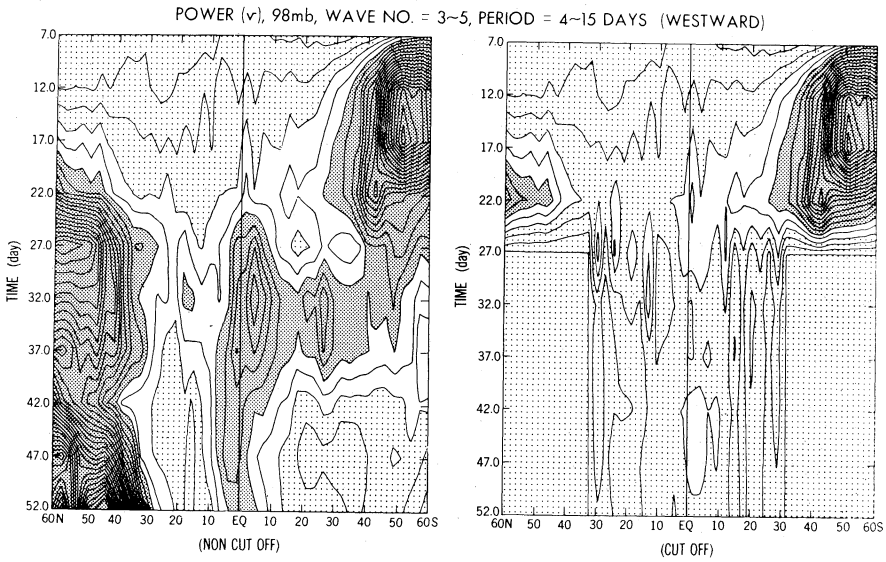

Fig. 15 Latitude-time sections (grid model, 98 mb) of the MEM power spectrum (wavenumbers 3~5, periods 4~15 days, westward moving) of the meridional component showing the results of control experiments. Small random disturbances are initially given on June 1 (left) and disturbances are eliminated poleward of 30° after June 20 (right). (15 days of the data are used for spectral analysis for every 5 day time increment.) Contour interval 0.25 $m^2 s^{-2}$. Dark shade>1.25, light shade<0.75. (After Hayashi and Golder, 1978).

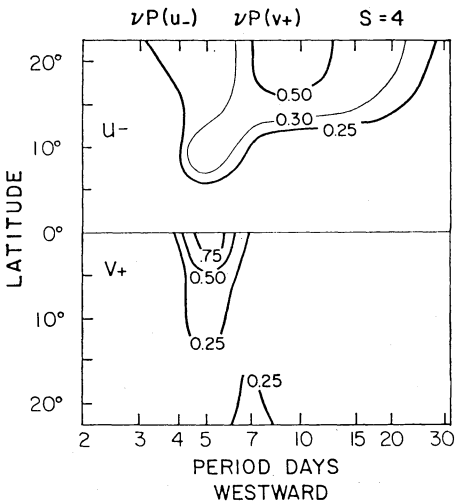

Fig. 16a Observed latitude-frequency distribution (200 mb, June-August, 1967) of the space-time power spectra (wavenumber 4) of winds. U_- indicates the half difference between the zonal components in both the hemispheres, while V_+ is the half sum of the meridional components. Spectral values are multiplied by frequency. (After Zangvil and Yanai, 1980).

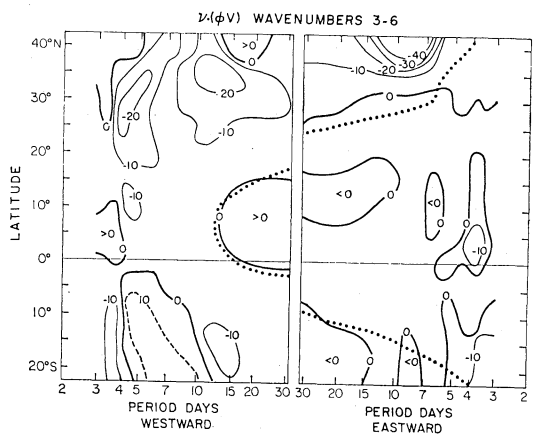

Fig. 16b Observed latitude-frequency distribution (200 mb, June-August, 1967) of the space-time spectra (wavenumbers 3~6) of the meridional flux of energy estimated through the Eliassen-Palm relation. (After Zangvil and Yanai, 1980).

and disturbances are eliminated computationally poleward of 30° after June 20 (right). Fifteen days of the data are used for spectral analysis for every 5 day time increment. It is seen that the kinetic energy of equatorial mixed Rossby-gravity waves are greatly reduced in the absence of mid-latitude disturbances.

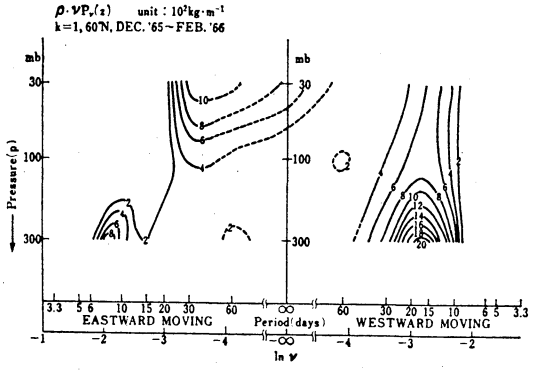

Fig. 17 Observed frequency-height distribution (60°N, December-February) of space-time power spectra (wavenumber 1) of the geopotential height. Spectral values are multiplied by air density and frequency. The left and right sides of the abscissa indicate eastward and westward moving periods. (After Sato, 1977).

As an example of the application of a space-time spectral analysis to observed data, Fig. 16 introduces a spectral analysis of mixed Rossby-gravity waves by Zangvil and Yanai (1980). Fig. 16a shows a latitude-frequency distribution at 200 mb of the space-time power spectra (wavenumber 4) of the half difference ($U-$) of the zonal components in both the hemispheres and the half sum ($V+$) of the meridional components. This procedure enhances vortices which are symmetric with respect to the equator. The $U-$ and $V+$ spectra at westward moving periods of 5 days attain their minimum and maximum, respectively, being in reasonable agreement with theoretical mixed Rossby-gravity mode. Fig. 16b shows a latitude-frequency distribution at 200 mb of the space-time spectra (wavenumber 3~6) of the meridional flux of energy estimated from the cospectra of the meridional flux of momentum through the Eliassen-Palm diagnostic relation. It is seen that energy is transported from the mid-latitudes toward the equatorial mixed Rossby-gravity waves with periods of 5 days.

3.2 *Analysis of mid-latitude waves*

The observed frequency-height distribution at 60°N of the space-time power spectra (wave-

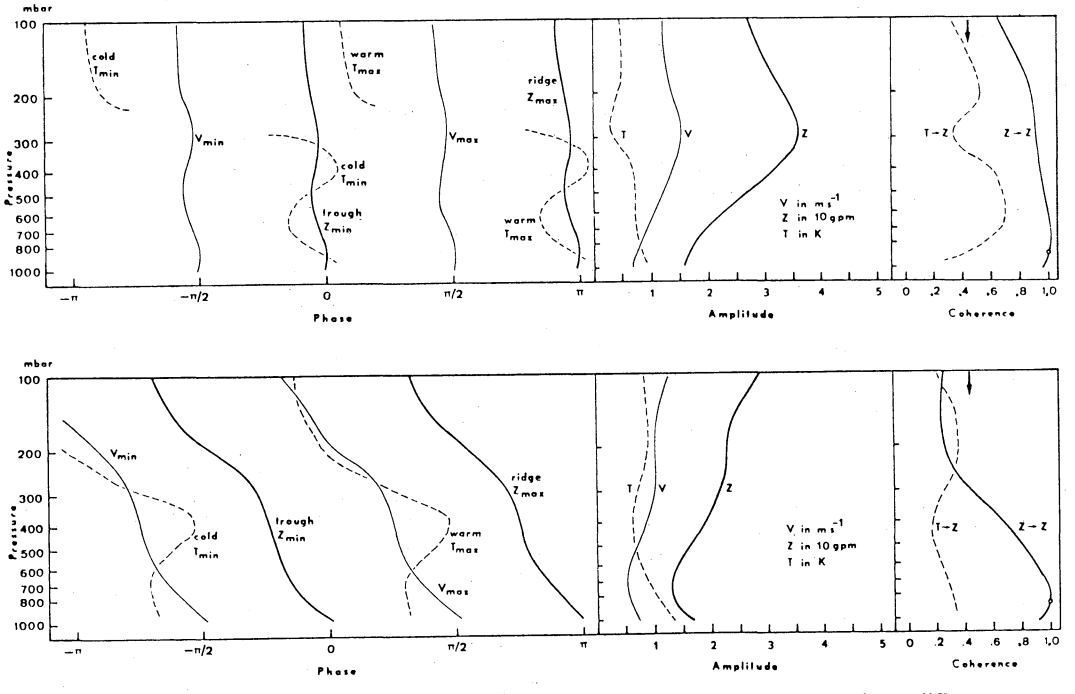

Fig. 18 Observed vertical distribution (50°N, winter of 1969~1970) of the phase difference (wavenumber 2, period 20 days), amplitude and the coherence with respect to the geopotential height at 800 mb. Westward (upper) and eastward (lower) moving waves. (After Böttger and Fraedrich, 1980).

number 1) of geopotential height is given in Fig. 17 (after Sato, 1977). It is seen that in the troposphere the westward moving component (right-hand side of the figure) is stronger than the eastward moving component, while in the stratosphere the eastward moving component is dominant.

Fig. 18 (after Böttger and Fraedrich, 1980) shows the observed vertical distributions (50°N) of the phase difference, amplitude and the coherence for westward (upper) and eastward (lower) moving components (wavenumber 2, period 20 days). It is seen that the westward moving component of the geopotential height has very little tilt in vertical, while the eastward moving component tilts westward with height. The amplitude of the westward moving com-

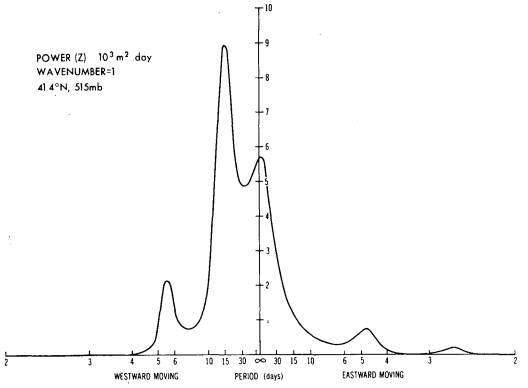

Fig. 19 Space-time spectral density (wavenumber 1) of the geopotential height (515 mb, 41.4°N) simulated by a GFDL spectral general circulation model. The maximum entropy method is used (after Hayashi, 1981b).

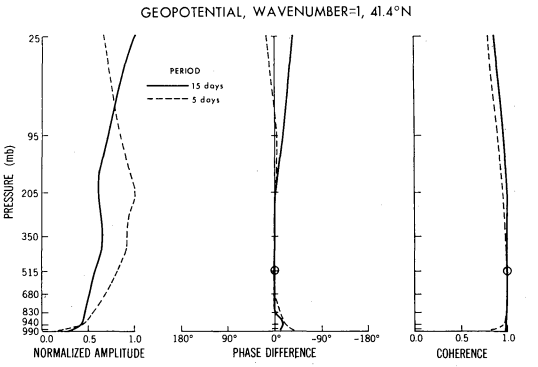

Fig. 20 Vertical distribution (spectral model, January, 41.4°N) of the normalized amplitude, phase difference and the coherence (geopotential height, wavenumber 1) with respect to the reference level 515 mb for westward moving periods of 15 (solid) and 5 (dashed) days. The maximum entropy method is used (after Hayashi, 1981b).

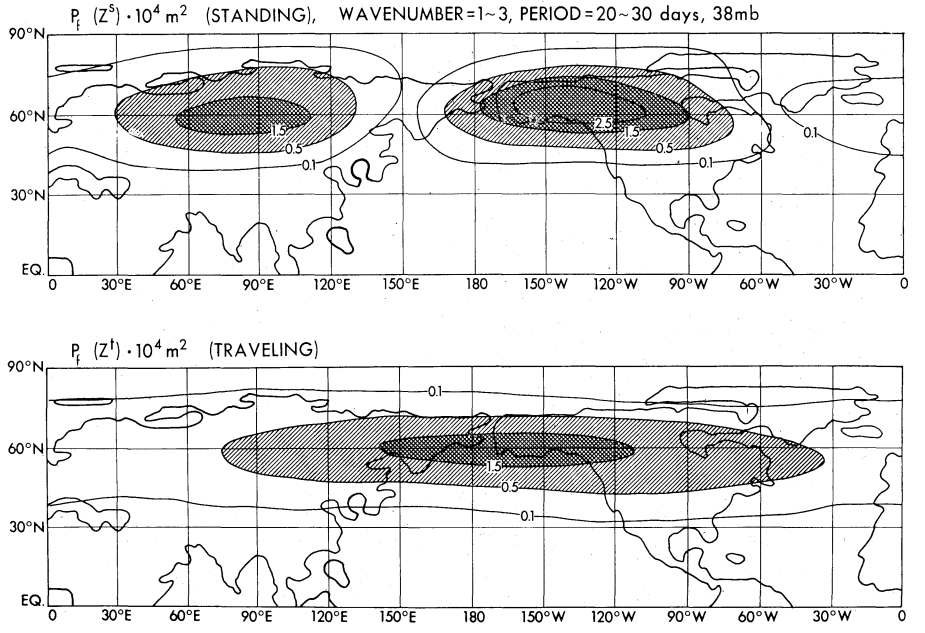

Fig. 21 Geographical distribution (grid model, 38 mb, October-March) of the time power spectra (period 20~30 days) of the geopotential height consisting of wavenumbers 1~3 for standing (upper) and traveling (lower) wave components. (After Hayashi, 1979b).

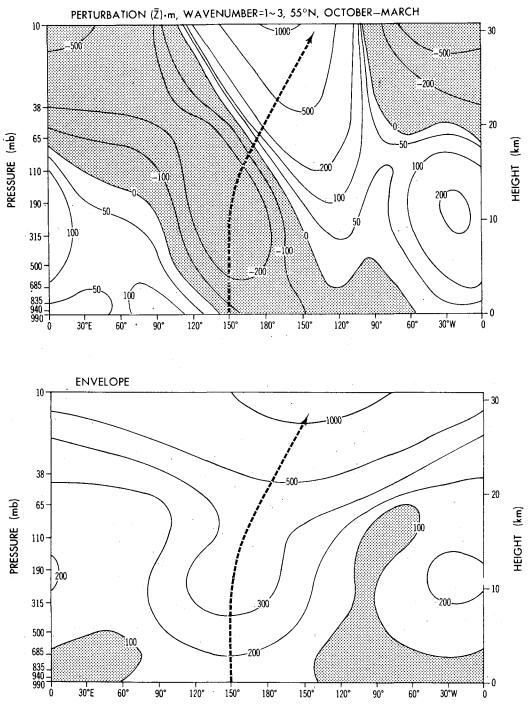

Fig. 22 Longitude-height section (grid model, 55°N, October-March) of the time mean geopotential height (upper) and its envelope (lower) consisting of wavenumbers 1~3. Dashed line indicates the position of the zonal maximum of the envelope. (After Hayashi, 1981a).

ponent decreases above 200 mb, while the eastward moving component increases. This suggests that the westward and eastward moving components correspond to external and internal Rossby waves, respectively, as has been pointed out by Pratt and Wallace (1976) based on an empirical orthogonal space-time cross spectral analysis.

The MEM space-time spectral density for wavenumber 1 of geopotential height (515 mb, 41.4°N, January) in Fig. 19 was simulated by a recent GFDL spectral general circulation model. Two spectral peaks are seen at westward moving periods of 15 and 5 days, corresponding to the observed external Rossby waves. The vertical structure of these simulated waves are displayed in Fig. 20. The amplitude is estimated by MEM power spectra, while phase difference and coherence are estimated by the MEM cross spectra. It is seen that these waves are characterized by little phase variation in vertical in agreement with observed waves.

As an example of the partition of transient waves into standing and traveling wave components (see Eq. 39), Fig. 21 shows the geographical distribution (38 mb) of the time power spectra (period 20~30 days) of the grid model's geopotential height consisting of wavenumbers 1~3. It is seen that the standing waves computed by (40) have two antinodes, over the Asian and North American continents, while the traveling waves, (41), attains only one maximum, over the Pacific. These traveling waves are dominated by eastward moving components and may correspond to those observed by Sato (1977).

Finally, an example of the application of the envelope analysis to stationary planetary waves is given. Fig. 22 displays the latitude-height section (grid model, 55°N) of the time mean geopotential height and its envelope (31) consisting of wavenumbers 1~3. It is seen that in the troposphere the envelope attains its major and minor maxima in the Pacific and Atlantic, respectively. The major maximum is dominated by wavenumbers 1~2 and shifts eastward with height in the direction of the group velocity in the stratosphere and strengthens the Aleutian high. This may explain why the Aleutian high stands out in the winter stratosphere.

4. Remarks

It is hoped that space-time spectral analysis methods which have been developed and refined for these 10 years will be more extensively and systematically applied to observed as well as simulated data. This should be possible by the advent of satellite observations, the Global Weather Experiment as well as general circulation models with an upper atmosphere. In particular, nonlinear energy transfer among the wavenumber-frequency components of atmospheric disturbances should be re-examined by use of the physically correct formulation of space-time spectral energy equations as discussed in Section 2.4.

Acknowledgments

The author would like to take this opportunity to express his hearty gratitude to Mr. D. G. Golder, collaborator, for his cooperation; to Dr. S. Manabe, supervisor, for his advice, and to Dr. J. Smagorinsky, director of GFDL, for his support of the research project. Dr. T. Maruyama has made valuable comments on the original manuscript. Thanks are extended to Ms. J. Kennedy for typing.

References

Bendat, J. S., and A. G. Piersol, 1971: Random Data: Analysis and Measurement Procedures. Wiley, 407 pp.

Born, M., and E. Wolf, 1975: Principles of Optics, 5th Ed. Pergamon Press, 808 pp.

Böttger, H. and K. Fraedrich, 1980: Disturbances in the wavenumber-frequency domain observed along 50°N. Contribution to *Atmos. Phys.*, **53**, 90-106.

Childers, D. G., 1978: Modern Spectrum Analysis. IEEE Press (reprint series), New York, 334 pp.

Deland, R. J., 1964: Traveling planetary waves. *Tellus*, **16**, 271-273.

————, 1972: On the spectral analysis of traveling waves. *J. Meteor. Soc. Japan*, **50**, 104-109.

Depradine, C. A., 1980: Energetics of large-scale motion in the tropics during GATE at 250 mb. *Mon. Wea. Rev.*, **108**, 886-895.

————, 1981: Waves at 200 mb during GATE. *Mon. Wea. Rev.*, **109**, 975-982.

Fraedrich, K., and H. Böttger, 1978: A wavenumber frequency analysis of the 500 mb geopotential at 50°N. *J. Atmos. Sci.*, **35**, 745-750.

Gruber, A., 1974: The wavenumber-frequency spectra of satellite measured brightness in the tropics. *J. Atmos. Sci.*, **31**, 1675-1680.

Hartmann, D. L., 1976: The structure of the stratosphere in the Southern Hemisphere during late winter 1973 as observed by satellite. *J. Atmos. Sci.*, **33**, 1141-1154.

Hayashi, Y., 1971: A generalized method of resolving disturbances into progressive and retrogressive waves by space Fourier and time cross-spectral analysis. *J. Meteor. Soc. Japan*, **49**, 125-128.

————, 1973: A method of analyzing transient waves by space-time cross spectra. *J. Appl. Meteor.*, **12**, 404-408.

————, 1974: Spectral analysis of tropical disturbances appearing in a GFDL general circulation model. *J. Atmos. Sci.*, **31**, 180-218.

————, 1977a: On the coherence between progressive and retrogressive waves and a partition of space-time power spectra into standing and traveling parts. *J. Appl. Meteor.*, **16**, 368-373.

————, 1977b: Space-time power spectral analysis using the maximum entropy method. *J. Meteor. Soc. Japan*, **55**, 415-420.

————, 1979a: Space-time spectral analysis of rotary vector series. *J. Atmos. Sci.*, **36**, 757-766.

————, 1979b: A generalized method of resolving transient disturbances into standing and traveling waves by space-time spectral analysis. *J. Atmos. Sci.*, **36**, 1017-1029.

————, 1980a: Estimation of nonlinear energy transfer spectra by the cross-spectral method. *J. Atmos. Sci.*, **37**, 299-307.

————, 1980b: A method of estimating space-time spectra from polar-orbiting satellite data. *J. Atmos. Sci.*, **37**, 1385-1392.

————, 1981a: Vertical-zonal propagation of a stationary planetary wave packet. *J. Atmos. Sci.*, **38**, 974-987.

————, 1981b: Space-time cross spectral analysis using the maximum entropy method. *J. Meteor. Soc. Japan*, **59**, 620-624.

————, 1982: Interpretations of space-time spectral energy equations. To appear in *J. Atmos. Sci.*, March.

————, and D. G. Golder, 1977: Space-time spectral analysis of mid-latitude disturbances appearing in a GFDL general circulation model. *J. Atmos. Sci.*, **34**, 237-262.

———— and ————, 1978: The generation of equatorial transient planetary waves: Control experiments with a GFDL general circulation model. *J. Atmos. Sci.*, **35**, 2068-2082.

———— and ————, 1980: The seasonal variation of tropical transient planetary waves appearing in a GFDL general circulation model. *J. Atmos. Sci.*, **37**, 705-716.

Hino, M., 1977: Spectral Analysis (in Japanese), Asakura Publishing Company, 300 pp. 162 Tokyo, Japan.

Iwashima, T., and R. Yamamoto, 1971: A method of separation of the ultra-long waves in the atmosphere into quasi-stationary and transient parts by the time filters. *J. Meteor. Soc. Japan*, **49**, 158-162.

Izawa, T., 1972: Some considerations on the continuous space-time spectral analysis of atmospheric disturbances. *Paper. Meteor. Geophys. Japan*, **23**, 33-71.

Jenkins, G. M., and D. G. Watts, 1968: Spectral Analysis and Its Applications. Holden-Day, 525 pp.

Kao, S. K., 1968: Governing equations and spectra for atmospheric motion and transports in frequency-wavenumber space. *J. Atmos. Sci.*, **25**, 32-38.

————, and H. N. Lee, 1977: The nonlinear interactions and maintenance of the large-scale moving waves in the atmosphere. *J. Atmos. Sci.*, **34**, 471-485.

————, 1980: Equations of kinetic and available potential energy evolution in wavenumber frequency space. *Pageoph.*, **118**, 867-879.

Krishnamurti, T. N., 1979: Large-scale features of the tropical atmosphere, in Meteorology of Tropical Oceans, Royal Meteorological Society, London.

————, and P. Ardanuy, 1980: The 10 to 20-day westward propagating mode and "Breaks in the Monsoons." *Tellus*, **32**, 15-26.

Manabe, S., D. G. Hahn and J. L. Holloway, Jr., 1974: The seasonal variation of the tropical circulation as simulated by a global model of the

atmosphere. *J. Atmos. Sci.*, **31**, 43-83.
————, ————, and ————, 1979: Climate simulations with GFDL spectral models of the atmosphere: Effect of truncation. GARP Publication Series, No. 22, Vol. 1, 41-94.
Miyakoda, K., A. Rosati, and F. E. Boland, 1981: The variation of sea surface temperature in 1976 and 1977. Part II. The characteristics of spatial and temporal variability. Submitted to *J. Geophys. Res.*
Mooers, C. N. K., 1973: A technique for the cross spectrum analysis of pairs of complexed-valued time series, with emphasis on properties of polarized components and rotational invariants. *Deep-Sea Res.*, **20**, 1129-1141.
Pan, H. L., 1979: Upper tropospheric tropical circulations during a recent decade. Department of Meteorology, Florida State University, Report No. FSU 79-1.
Pratt, R. W., 1976: The interpretation of space-time spectral quantities. *J. Atmos. Sci.*, **33**, 1060-1066.
————, 1977: Space-time kinetic energy spectra in mid-latitude. *J. Atmos. Sci.*, **34**, 1054-1057.
————, 1979: A space-time spectral comparison of the NCAR and GFDL general circulation models to the atmosphere. *J. Atmos. Sci.*, **36**, 1681-1691.
————, and J. M. Wallace, 1976: Zonal propagation characteristics of large-scale fluctuations in the mid-latitude troposphere. *J. Atmos. Sci.*, **33**, 1184-1194.
Saltzman, B., 1957: Equations governing the energetics of the large scales of atmospheric turbulence in the domain of wavenumber. *J. Meteor.*, **14**, 513-523.
Sato, Y., 1977: Transient planetary waves in the winter stratosphere. *J. Meteor. Soc. Japan*, **55**, 89-106.
Shäfer, J., 1979: A space-time analysis of tropospheric planetary waves in the Northern Hemisphere. *J. Atmos. Sci.*, **36**, 1117-1123.
Straus, D. M., and J. Shukla, 1981: Space-time spectral structure of a GLAS general circulation model and a comparison with observations. *J. Atmos. Sci.*, **38**, 902-917.
Tsay, C. Y., 1974: A note on the methods of analyzing traveling waves. *Tellus*, **26**, 412-415.
Ulrych, T. J. and T. N. Bishop, 1975: Maximum entropy spectral analysis and autoregressive decomposition. *Rev. of Geophys. and Space Phys.*, **13**, 183-200.
Venne, D. E., and J. L. Stanford, 1979: Observation of a 4-day temperature wave in the polar winter stratosphere. *J. Atmos. Sci.*, **36**, 2016-2019.
Yanai, M., and T. Maruyama, 1966: Stratospheric wave disturbances propagating over the equatorial Pacific. *J. Meteor. Soc. Japan*, **44**, 291-294.
Zangvil, A., 1975: Temporal and spatial behavior of large-scale disturbances in tropical cloudiness deduced from satellite brightness data. *Mon. Wea. Rev.*, **103**, 904-920.
————, and M. Yanai, 1980: Upper tropospheric waves in the tropics. Part I: Dynamical analysis in the wavenumber-frequency domain. *J. Atmos. Sci.*, **37**, 283-298.
———— and ————, 1981: Upper tropospheric waves in the tropics. Part II: Association with clouds in the wavenumber-frequency domain. *J. Atmos. Sci.*, **38**, 939-953.

時空間スペクトル解析法と大気波動への応用

林　　良　一
GFDL, Princeton University, U.S.A.

時空間スペクトル解析法と大気大規模波動への応用を評論した。

時空間スペクトル解析は非定常波を東進と西進成分に分解し，二次元速度ベクトルを時計的と反時計的回転成分に分解する回転スペクトル解析法と数学的に類比している。時空間スペクトル解析法により複数の波数から構成されている非定常波を停滞波と移動波の波束に分解することも可能である。時空間エネルギー・スペクトルは時空間スペクトルエネルギー方程式により支配され，線型と非線型エネルギー分配スペクトルにより波数振動数空間での再分配が表現される。

時空間スペクトルは時系列データの長さに応じて相関法，直接フーリエ変換法及び最大エントロピー法により推定される。空間フーリエ変換を修正することにより極軌道衛星による非同時観測データからも正確に時空間スペクトルが求められる。

時空間スペクトル解析法を GFDL 大気大循環モデルと観測との比較や制御実験の解析に応用することにより大気大規模擾乱の波動特性，構造，エネルギー収支，発生機構などが明らかになってきた。